

aminocarbonyl ligand. Examples of triply bridging aminocarbonyl ligands have also been reported.¹⁷ We cannot distinguish between these processes at this time. Another important step in the transformation is the conversion of the iminium ligand into a bridging ligand. It is proposed that this occurs by a cleavage of the osmium-nitrogen bond to produce an aminomethyl ligand. Such a transformation has been reported previously.⁸ In the present case, the transformation would be assisted by the addition of a mole of CO from the environment. Nucleophilic attack of the amino group on the appropriate neighboring metal atom could induce loss of a CO ligand and complete the formation of the bridge. The transformation would occur similarly via either of the proposed intermediates B or C. To complete the formation of 4 an additional CO ligand

must be acquired at atom Os(3) and one must be eliminated from Os(2). This could be accomplished most easily by an intramolecular shift involving a bridging CO ligand but could have occurred alternatively by a dissociation/addition process.

Acknowledgment. These studies were supported by the Office of Basic Energy Sciences of the U.S. Department of Energy. We wish to thank Johnson Matthey Inc. for a loan of osmium tetroxide. The Bruker AM-300 NMR spectrometer was purchased with funds from the National Science Foundation under Grant No. CHE-8411172.

Registry No. ³, 106906-16-5; 4, 106906-17-6; 5, 106906-15-4; CH₂(NMe₂)₂, 51-80-9.

Supplementary Material Available: Tables of anisotropic thermal parameters for 4 and 5 (4 pages); structure factor amplitudes for compounds 4 and 5 (46 pages). Ordering information is given on any current masthead page.

(17) Seyferth, D.; Hallgren, J. E.; Hung, P. L. K. *J. Organomet. Chem.* 1973, 50, 265.

Linear Chain Organometallic Donor-Acceptor Complexes and One-Dimensional Alloys. Synthesis and Structure of $[(\eta^6\text{-C}_6\text{Me}_3\text{H}_3)_2\text{M}][\text{C}_6(\text{CN})_6]$ (M = Fe, Ru)

Michael D. Ward

Central Research and Development Department, E. I. du Pont de Nemours & Co., Experimental Station, Wilmington, Delaware 19898

Received July 18, 1986

Organometallic linear chain complexes $[(\eta^6\text{-C}_6\text{Me}_3\text{H}_3)_2\text{M}][\text{C}_6(\text{CN})_6]$ (M = Fe, **1a**; M = Ru, **2a**) and $[(\eta^6\text{-C}_6\text{Me}_6)_2\text{M}][\text{C}_6(\text{CN})_6]$ (M = Fe, **1b**; M = Ru, **2b**) prepared from $[(\eta^6\text{-arene})_2\text{M}]^{2+}$ cations and $[\text{C}_6(\text{CN})_6]^{2-}$ are described. Single-crystal X-ray studies show that **1a** crystallizes in the space group $R\bar{3}$, with $a = 14.875$ (5) Å, $c = 9.858$ (4) Å, $V = 1889$ (2) Å³, $\rho = 1.38$ g cm⁻³, $Z = 3$, $R_u = 0.047$, and $R_w = 0.056$. The ruthenium analogue **2a** also crystallizes in the space group $R\bar{3}$, with $a = 14.825$ (5) Å, $c = 10.093$ (3) Å, $V = 1921$ (2) Å³, $\rho = 1.48$ g cm⁻³, $Z = 3$, $R_u = 0.026$, and $R_w = 0.031$. Both complexes exhibit mixed stacks of alternating cations and anions with interplanar spacings less than the sum of the van der Waals radii. The complexes exhibit strong charge-transfer bands and are best described as "superionic" donor-acceptor (DA) complexes with nominally doubly charged ($\text{D}^{2-}\text{A}^{2+}$) ground states and (D^-A^+) excited states. The difference in the charge-transfer absorption energies for a given donor dianion is equivalent to the difference in the reduction potentials of the isostructural $[(\eta^6\text{-arene})_2\text{M}]^{2+}$ cations in solution. Since **1a** and **2a** both crystallize in the $R\bar{3}$ space group and exhibit different unit cell lengths along only the linear chain axis, mixed-metal linear chain complexes $[(\eta^6\text{-C}_6\text{Me}_3\text{H}_3)_2\text{Fe}]_x[(\eta^6\text{-C}_6\text{Me}_3\text{H}_3)_2\text{Ru}]_{1-x}[\text{C}_6(\text{CN})_6]$ are readily prepared. These mixed-metal phases exhibit optical absorption intensities consistent with Beer's law behavior, and the macroscopic optical properties can be tailored by control of the relative amounts of the iron and ruthenium chromophores.

Introduction

Molecular solids, and particularly quasi-one-dimensional (1-D) materials, have been the subject of intensive investigation owing to their unique and interesting properties,¹ as well as their potential for electronic applications.² Design of new molecular solids relies on better understanding of the structure-property relationships as well as new concepts for rational modification of physical properties. Although most studies have focused upon electrical and magnetic behavior, investigation of optical

properties can also lend insight into the solid-state properties of 1-D materials. In particular, behavior associated with Mulliken charge-transfer (CT) interactions between π -donors and π -acceptors³⁻⁵ allows one to explore the nature of donor-acceptor (DA) interactions in mixed-stack solids.

In an effort to further understand the properties of low-dimensional solids, we have sought to prepare new materials that incorporate organometallic components. The design of new one-dimensional materials using or-

(1) *Extended Linear Chain Compounds*; Miller, J. S., Ed.; Plenum: New York, 1981-1983.

(2) (a) *Molecular Semiconductors*; Lehn, J. M.; Rees, Ch. W. Eds.; Springer-Verlag: New York, 1985. (b) *Molecular Electronic Devices*; Carter, F., Ed.; Dekker: New York, 1982.

(3) Mulliken, R. S.; Person, W. B. *Molecular Complexes: A Lecture and Reprint Volume*; Wiley: New York, 1969.

(4) Soos, Z. G. *Annu. Rev. Phys. Chem.* 1974, 25, 121.

(5) Andrews, L. J.; Keefer, R. M. *Molecular Complexes in Organic Chemistry*; Holden-Day: San Francisco, CA, 1964.

ganometallic reagents is particularly attractive since the diverse variety of these compounds may afford materials with unusual electronic properties. Although mixed-stack donor-acceptor complexes with organometallic components have not been extensively reported, the one-dimensional phases $[(\eta^5\text{-C}_5\text{H}_5)_2\text{Fe}][\text{TCNE}]$,⁶ $[(\eta^5\text{-C}_5\text{Me}_5)_2\text{Fe}]^+[\text{TCNQ}]^-$,⁷ $[(\eta^5\text{-C}_5\text{Me}_5)_2\text{Fe}]^+[\text{TCNE}]^-$,⁸ and $[(\eta^5\text{-C}_5\text{Me}_5)_2\text{Fe}]^+[\text{DDQ}]^-$ ⁹ (TCNE = tetracyanoethylene, DDQ = dichlorodicyanoquinodimethane, TCNQ = tetracyanoquinodimethane) illustrate that organometallic components with planar, aromatic ring systems are among the most likely candidates to mimic organic DA complexes. The ligand environment and dipositive charge of $[(\eta^6\text{-arene})_2\text{M}]^{2+}$ cations^{10,11} (M = Fe, Ru; arene = hexamethylbenzene, mesitylene) suggested that these species may be models for aromatic organic dications,¹² thereby permitting the investigation of mixed-stack DA solids with doubly charged ground states. Little is known about the structural aspects of this class of DA solids owing to the paucity of organic dications and dianions, as only one example, $[\text{N,N-dimethylbipyridinium}]^{2+}[\text{iso-C}_4(\text{CN})_6]^{2-}$,¹³ has been reported. Furthermore, the reports^{14,15} that $[(\eta^6\text{-arene})_2\text{M}]^{1+}$ and $[(\eta^6\text{-arene})_2\text{M}]^0$ are attainable via chemical and electrochemical reduction of the dication suggested that materials derived from these species may exhibit interesting properties arising from charge transfer in the solid state.

We report herein the synthesis and structural characterization of novel one-dimensional, organometallic DA solids prepared from $[(\eta^6\text{-arene})_2\text{M}]^{2+}$ (M = Fe, Ru) and hexacyanotrimethylenecyclopropane dianion, $[\text{C}_6(\text{CN})_6]^{2-}$.¹⁶ These phases exhibit classical Mulliken donor-acceptor behavior analogous to that of organic complexes but are "superionic"¹⁷ in that the ground states possess donors and acceptors that nominally are doubly charged. Their CT absorption energies depend upon the identity of the metal and can be correlated with ΔE_{redox} of the organometallic cations. Additionally, their macroscopic optical properties can be tailored by the formation of one-dimensional "organometallic alloys" that contain mixed-metal linear chains of donor-acceptor pairs.

Results and Discussion

Synthesis and Structure of $[(\eta^6\text{-Arene})_2\text{M}][\text{C}_6(\text{CN})_6]$. Although the physical and electronic properties of bis(arene)iron and -ruthenium complexes have been extensively investigated, their structural properties and role as components in CT complexes have not been ex-

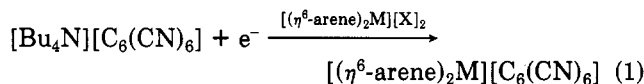
Table I. Bond Distances (Å) in $[(\eta^6\text{-C}_6\text{Me}_3\text{H}_3)_2\text{M}][\text{C}_6(\text{CN})_6]$ Complexes^a

1a		2a	
atoms	dist	atoms	dist
Fe-C1	2.101 (4)	Ru-C1	2.215 (3)
Fe-C2	2.126 (4)	Ru-C2	2.242 (3)
N1-C6	1.11 (1)	N1-C6	1.120 (6)
N1-C7	1.09 (1)	N1-C7	1.112 (9)
C1-C2	1.401 (5)	C1-C2	1.414 (5)
C1-C2	1.411 (5)	C1-C2	1.416 (4)
C1-H1	0.95 (3)	C1-H2	0.94 (5)
C2-C3	1.505 (6)	C2-C3	1.493 (3)
C3-H2	0.97 (5)	C3-H2	1.02 (5)
C3-H3	1.10 (7)	C3-H3	1.06 (4)
C3-H4	0.96 (6)	C3-H4	0.95 (5)
C4-C4	1.38 (1)	C4-C4	1.387 (10)
C4-C5	1.39 (1)	C4-C5	1.398 (7)
C5-C6	1.42 (1)	C5-C6	1.409 (8)
C5-C7	1.42 (1)	C5-C7	1.406 (11)

^a Numbers in parentheses are estimated standard deviations in the least significant digits.

plored. Charge-transfer complexes are commonly prepared by in situ electron-transfer routes involving an oxidizable donor and a reducible acceptor. However, synthesis of new DA complexes via metathesis techniques using the 18-electron $[(\eta^6\text{-arene})_2\text{M}]^{2+}$ dications seemed more desirable as these species are very robust compared to their more highly reduced analogues. This obviously requires the presence of a suitable dianion, preferably one with a planar geometry in order to facilitate molecular packing. The hexacyanotrimethylenecyclopropane (HTMCP) dianion,¹⁶ $[\text{C}_6(\text{CN})_6]^{2-}$, fulfills these qualifications and exhibits D_{3h} symmetry, which seemed particularly well suited to the symmetry of the arene ligands of $[(\eta^6\text{-arene})_2\text{M}]^{2+}$.

When acetonitrile (or nitromethane) solutions of $[\text{Bu}_4\text{N}]_2[\text{C}_6(\text{CN})_6]$ were added to acetonitrile (or nitromethane) solutions of $[(\eta^6\text{-C}_6\text{Me}_3\text{H}_3)_2\text{Fe}][\text{PF}_6]_2$ or $[(\eta^6\text{-C}_6\text{Me}_6)_2\text{Fe}][\text{PF}_6]_2$, dark blue, air-stable microcrystalline $[(\eta^6\text{-C}_6\text{Me}_3\text{H}_3)_2\text{Fe}][\text{C}_6(\text{CN})_6]$ (**1a**) or $[(\eta^6\text{-C}_6\text{Me}_6)_2\text{Fe}][\text{C}_6(\text{CN})_6]$ (**1b**) immediately precipitated. Similar methods also afforded $[(\eta^6\text{-C}_6\text{Me}_3\text{H}_3)_2\text{Ru}][\text{C}_6(\text{CN})_6]$ (**2a**) or $[(\eta^6\text{-C}_6\text{Me}_6)_2\text{Ru}][\text{C}_6(\text{CN})_6]$ (**2b**) as microcrystalline orange-red powders. Alternatively, **1a,b** and **2a,b** were prepared electrochemically by reduction of $[\text{C}_6(\text{CN})_6]^{2-}$ in the presence of $[(\eta^6\text{-arene})_2\text{M}]^{2+}$ (eq 1).



Single crystals of **1a** and **2a** were grown by slow diffusion methods since their negligible solubility precluded the use of conventional recrystallization methods. The single-crystal X-ray structures were solved for the mesitylene complexes, which generally tended to form larger, more tractable crystals. The hexamethylbenzene analogues were generally plagued by twinning and solvent loss, which prevented their structural analysis.

Single-crystal X-ray diffraction revealed that **1a** and **2a** both crystallize in the space group $R\bar{3}$ and possess linear chains with alternating $[(\eta^6\text{-C}_6\text{Me}_3\text{H}_3)_2\text{M}]^{2+}$ cations and $[\text{C}_6(\text{CN})_6]^{2-}$ anions (Figure 1). The bond distances and angles of the cation are as expected (Tables I and II; Figure 2), and those of **1a** are similar to those observed in the $[(\eta^6\text{-C}_6\text{Me}_3\text{H}_3)_2\text{Fe}]^{2+}$ cation in $[(\eta^6\text{-C}_6\text{Me}_3\text{H}_3)_2\text{Fe}][\text{C}_6(\text{CN})_6]_2$.¹⁸ The central metal atoms lie at an inversion center; thus the mesitylene rings are staggered with respect to each other. The average $C_{\text{ring}}-C_{\text{ring}}$ distances are as one

(6) Rosenblum, M.; Fish, R. W.; Bennett, C. *J. Am. Chem. Soc.* **1964**, *86*, 5166.

(7) Candela, G. A.; Swarzendruber, L.; Miller, J. S.; Rice, M. J. *J. Am. Chem. Soc.* **1979**, *101*, 2755.

(8) Miller, J. S.; Calabrese, J. C.; Epstein, A. J.; Bigelow, R. W.; Zhang, J. H.; Reiff, W. M. *J. Chem. Soc., Chem. Commun.* **1986**, 1026.

(9) Gerbert, E.; Reis, A. H., Jr.; Miller, J. S.; Rommelmann, H.; Epstein, A. *J. Am. Chem. Soc.* **1982**, *104*, 4403.

(10) Helling, J. F.; Braitsch, D. M. *J. Am. Chem. Soc.* **1970**, *92*, 7207.

(11) Bennett, M. A.; Matheson, T. W. *J. Organomet. Chem.* **1979**, *175*, 87.

(12) (a) Weiss, R.; Schloter, K. *Tetrahedron Lett.* **1975**, *16*, 3491. (b) Johnson, R. W. *Tetrahedron Lett.* **1976**, *17*, 589. (c) Bechgaard, K.; Parker, V. D. *J. Am. Chem. Soc.* **1972**, *94*, 4749. (d) Gerson, F.; Plattner, G.; Yoshida, Z. *Mol. Phys.* **1971**, *21*, 1027.

(13) Nakamura, K.; Kai, Y.; Yasuoka, N.; Kasai, N. *Bull. Chem. Soc. Jpn.* **1981**, *54*, 3300.

(14) Michaud, P.; Mariot, J.-P.; Varret, F.; Astruc, D. *J. Chem. Soc., Chem. Commun.* **1982**, 1383.

(15) (a) Finke, R. G.; Voegeli, R. H.; Laganis, E. D.; Boekelheide, V. *Organometallics* **1983**, *2*, 347. (b) Laganis, E. D.; Voegeli, R. H.; Swann, R. T.; Finke, R. G.; Hopf, H.; Boekelheide, V. *Organometallics* **1982**, *1*, 11.

(16) Fukunaga, T. *J. Am. Chem. Soc.* **1976**, *98*, 610.

(17) Strebel, P. J.; Soos, Z. G. *J. Chem. Phys.* **1970**, *53*, 4077.

(18) Miller, J. S.; Ward, M. D., manuscript in preparation.

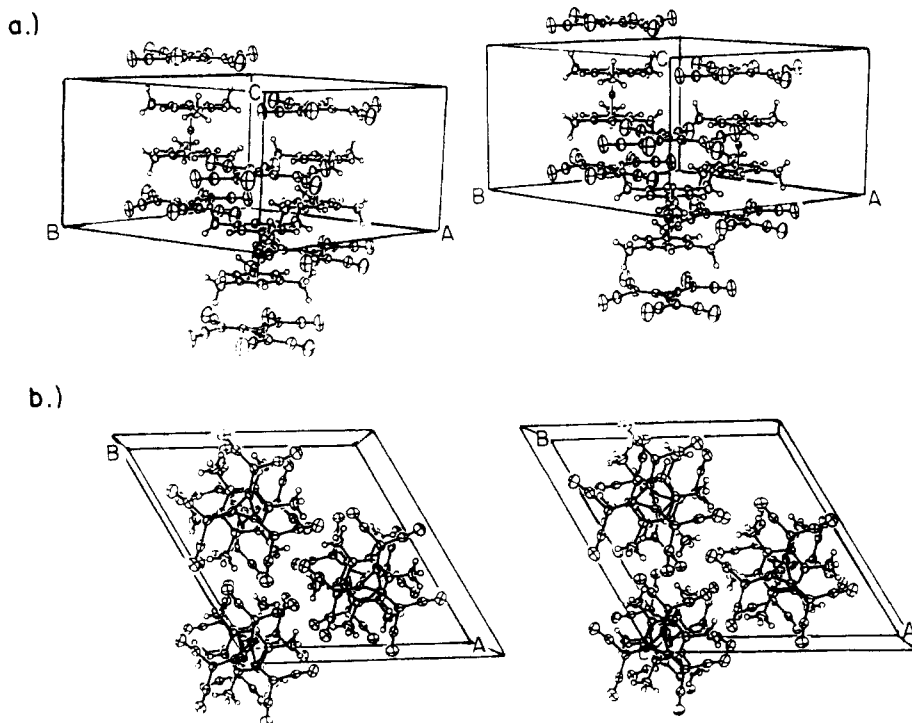


Figure 1. Stereoviews of the unit cell of **1a** as viewed down the (a) *a* axis and (b) *c* axis. The atoms are displayed with 50% ellipsoids.

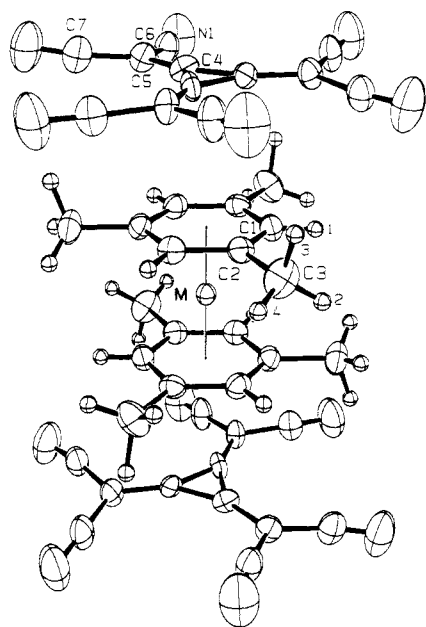


Figure 2. Numbering scheme for the $[(\eta^6\text{-C}_6\text{Me}_3\text{H}_3)_2\text{M}][\text{C}_6(\text{CN})_6]$ ion pair in **1a** and **2a**.

would expect for mesitylene, with an average value of 1.405 (5) and 1.415 (5) Å for **1a** and **2a**, respectively. The rings are essentially planar, although the M–C bond distances to the methyl substituted carbons are slightly longer than the M–C distances to the unsubstituted ring carbons. The methyl groups are only slightly bent out of the ring plane away from the central metal atom by 0.010 Å in **1a** and 0.024 Å in **2a**. The M–C distances are larger in **1a** than in **2a** due to the larger radius of Ru^{II} ,¹⁹ resulting in a larger separation between the intramolecular mesitylene rings in the latter (i.e., **1a**, 3.16 Å; **2a**, 3.44 Å). Accordingly, the iron and ruthenium atoms are located 1.58 and 1.72 Å from

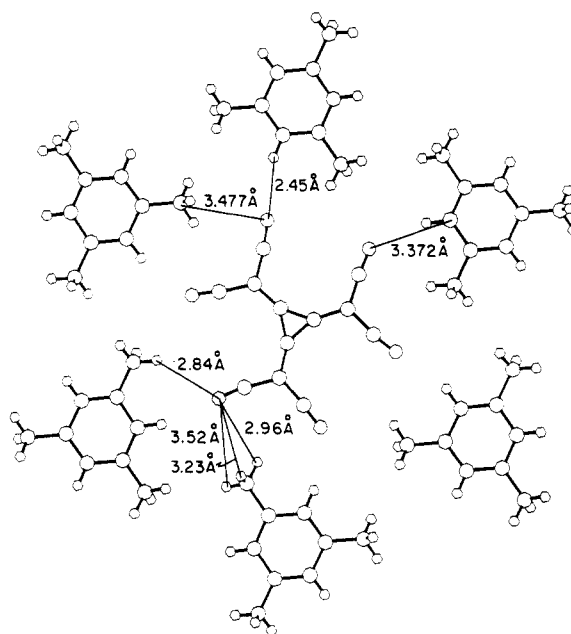


Figure 3. Intermolecular contacts in the two-dimensional sheets of anions and cations in **1a** and **2a**. The anion lies nearly in a plane defined by six neighboring mesitylene rings belonging to the $[(\eta^6\text{-C}_6\text{Me}_3\text{H}_3)_2\text{M}]^{2+}$ cations. The closest intermolecular contacts are observed between N1 and H1 and between N1 and C1.

the planes of the mesitylene rings, respectively. The difference in the interligand distances is similar to that between $[(\eta^5\text{-C}_5\text{Me}_5)_2\text{Fe}]$ ²⁰ and $[(\eta^5\text{-C}_5\text{Me}_5)_2\text{Ru}]$,²¹ which exhibit values of 3.314 and 3.616 Å, respectively.

The most distinguishing feature of the dianion is the short $C_{\text{ring}}\text{-}C_{\text{ring}}$ distance of 1.39 Å (Table III), which is significantly shorter than the analogous bond distance in

(19) Shannon, R. D. *Acta Crystallogr., Sect. A: Cryst. Phys., Diffraction, Theor. Gen. Crystallogr.* 1976, A32, 751.

(20) Struchkov, Yu. T.; Andrianov, V. G.; Sal'nikova, T. N.; Lyatfiov, I. R.; Materikova, R. B. *J. Organomet. Chem.* 1978, 145, 213.

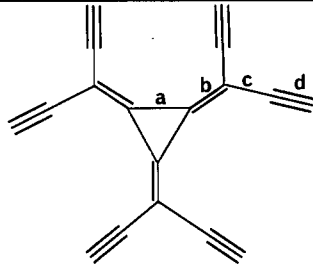
(21) Liles, D. C.; Shaver, A.; Singleton, E.; Wiege, M. B. *J. Organomet. Chem.* 1985, 282, C33.

Table II. Bond Angles (deg) in $[(\eta^6\text{-C}_6\text{Me}_3\text{H}_3)_2\text{M}][\text{C}_6(\text{CN})_6]^\text{c}$

atoms	angle		atoms	angle	
	1a (M = Fe)	2a (M = Ru)		1a (M = Fe)	2a (M = Ru)
C1-M-C1	70.2 (2)	66.4 (1)	C1-C2-C3	121.0 (4)	120.9 (3)
C1-M-C1	180.00	180.00	C1-C2-M	69.7 (2)	70.5 (2)
C1-M-C1	109.8 (2)	113.6 (1)	C1-C2-C3	120.6 (4)	120.9 (3)
C1-M-C2	38.7 (1)	37.0 (1)	C1-C2-M	69.5 (2)	70.5 (2)
C1-M-C2	39.0 (1)	37.0 (1)	C3-C2-M	131.2 (3)	128.4 (2)
C1-M-C2	83.4 (1)	78.8 (1)	C2-C3-H2	112 (3)	111 (2)
C1-M-C2	141.3 (1)	143.0 (1)	C2-C3-H3	108 (3)	109 (2)
C1-M-C2	141.0 (1)	143.0 (1)	C2-C3-H4	117 (3)	116 (2)
C1-M-C2	96.6 (1)	101.2 (1)	H2-C3-H3	111 (4)	116 (4)
C2-M-C2	70.5 (2)	67.0 (1)	H2-C3-H4	106 (4)	106 (4)
C2-M-C2	180.00	180.00	H3-C3-H4	102 (5)	98 (4)
C2-M-C2	109.5 (2)	113.0 (1)	C4-C4-C4	60.00	59.7 (8)
H1-C1-C2	121 (2)	120 (3)	C4-C4-C5	145.0 (4)	143.3 (9)
H1-C1-C2	117 (2)	118 (3)	C4-C4-C5	155.0 (4)	156.7 (9)
H1-C1-M	129 (2)	128 (3)	C4-C5-C6	118.0 (2)	123.0 (7)
C2-C1-C2	121.6 (4)	121.9 (3)	C4-C5-C7	124.0 (2)	119.1 (6)
C2-C1-M	71.6 (2)	72.5 (2)	N1-C6-C5	172.0 (1)	172.4 (8)
C2-C1-M	71.5 (2)	72.5 (2)	N1-C7-C5	173.0 (1)	172.1 (7)
C1-C2-C1	118.4 (4)	118.1 (2)			

^c Numbers in parentheses are estimated standard deviations in the least significant digits.

Table III. Average Bond Lengths (Å) in $\text{C}_6(\text{CN})_6^{2-}$ Anions^c

complex	n				
		a $\text{C}_{\text{ring}}\text{-C}_{\text{ring}}$	b $\text{C}_{\text{ring}}\text{-C}_{\text{exo}}$	c C-C	d C-N
$[(\eta^6\text{-C}_6\text{H}_3\text{Me}_3)_2\text{Fe}][\text{C}_6(\text{CN})_6]$	2	1.38 (1)	1.39 (1)	1.42 (1)	1.10 (1)
$[(\eta^6\text{-C}_6\text{H}_3\text{Me}_3)_2\text{Ru}][\text{C}_6(\text{CN})_6]$	2	1.387 (10)	1.398 (7)	1.407 (10)	1.116 (8)
$[(\eta^6\text{-C}_6\text{H}_3\text{Me}_3)_2\text{Fe}][\text{C}_6(\text{CN})_6]_2^\text{c}$	1	1.40 (1)	1.37 (1)	1.42 (1)	1.146 (9)
$[(\eta^5\text{-C}_5\text{Me}_5)_2\text{Fe}][\text{C}_6(\text{CN})_6]^\text{c}$	1	1.385 (12)	1.383 (12)	1.437 (10)	1.126 (8)
$[\text{Bu}_4\text{N}][\text{C}_6(\text{CN})_6]^\text{c,d}$	1				
$[\text{Bu}_4\text{N}]_2[\text{C}_6(\text{CN})_6]$	2	1.385 (15)	1.394 (15)	1.418 (15)	1.16 (3)
cyclopropane ^b		1.514 (2)			

^a Numbers in parentheses are estimated standard deviations in the least significant digits. ^b Reference 22. ^c Reference 18. ^d The bond lengths and angles of the monoanion in $[\text{Bu}_4\text{N}][\text{C}_6(\text{CN})_6]$ have not been determined. However, those reported for $[(\eta^6\text{-C}_6\text{H}_3\text{Me}_3)_2\text{Fe}][\text{C}_6(\text{CN})_6]_2$ and $[(\eta^5\text{-C}_5\text{Me}_5)_2\text{Fe}][\text{C}_6(\text{CN})_6]$ probably suffice.

cyclopropane.²² The average $\text{C}_{\text{ring}}\text{-C}_{\text{exo}}$ distance of 1.38 Å is slightly longer than the double bond length in ethylene (1.34 Å). The anion is essentially planar, although there is a slight twisting of the $\text{C}(\text{CN})_2$ group (ca. 6.6°) out of the cyclopropane ring plane. The structural parameters of the anion are essentially identical with those of the isolated dianion in $[\text{Bu}_4\text{N}]_2[\text{C}_6(\text{CN})_6]$,¹⁸ with the exception of a shorter $\text{C}\equiv\text{N}$ bond length in **1a** and **2a**. This may be due to the solid-state packing of the ion pairs in which each anion is surrounded by six coplanar mesitylene ligands (Figure 3), which results in two-dimensional sheets of anions and mesitylene rings and close interstack contacts between N1-H1 (2.45 Å) and N1-C1 (3.372 Å). This arrangement probably results from strong electrostatic attraction between the ion pairs and obviates repulsive Coulombic interactions between anions.

The anion and mesitylene ring planes within a given stack are parallel with interplanar separations less than the usual 3.5–3.6-Å van der Waals separation²³ (i.e., **1a**, 3.29 Å; **2a**, 3.26 Å). The small difference in interplanar separations of **1a** and **2a** is believed to be due to the lower temperature during data collection for **2a**. Significant contraction of the unit cell dimensions as the temperature is lowered from +20 to -160°C was observed (Figure 4); the higher compressibility of the 1-D axis was made manifest in a greater change in the *c* axis over this temperature range compared to the *a* axis. Unit cell determinations for **1a** and **2a** at identical temperatures showed that the difference in *c* axis lengths was equivalent to the difference in the intramolecular mesitylene-mesitylene separation, suggesting that the interplanar distances are identical at the same temperature. The D_{3h} anion is symmetrically disordered about a site of $\bar{3}$ symmetry. As a result of the anion disorder the *exo*-methylene groups exhibit both slightly slipped "eclipsed" and "staggered" conformations with respect to the methyl groups of the neighboring mesitylene rings. The $\text{C}_{\text{ring}}\text{-C}_{\text{exo}}$ bond of the anion does not lie directly over the axis of the $\text{C-H}_{(\text{ring})}$ bond (or C-CH_3) but is displaced by 10.1° as viewed down the 1-D *c* axis. The interior C1-C4 and C1-C5 distances are nearly equivalent (3.36 and 3.38 Å, respectively). This conformation appears to minimize steric interaction between methyl hydrogens and $\text{C}(\text{CN})_2$ groups.

(22) W. R. Jones; B. P. Stoicheff *Can. J. Phys.* 1964, 42, 2259.

(23) Bondi, A. *J. Phys. Chem.* 1964, 68, 441.

Table IV. Electrochemical and Spectroscopic Data for 1 and 2

complex	visible		IR ν_{CN} , cm^{-1}	cation	$E^{\circ 2+/1+}$, V vs. SCE
	$h\nu_{\text{CT}}$, cm^{-1}	$h\nu_{\text{CT}}$, eV			
1a	13 700	1.69	2169, 2189	$[(\eta^6\text{-C}_6\text{H}_3\text{Me}_3)_2\text{Fe}]^{2+}$	+0.02 ^a
1b	12 560	1.55	2169, 2188	$[(\eta^6\text{-C}_6\text{Me}_6)_2\text{Fe}]^{2+}$	-0.24
2a	19 888	2.46	2170, 2189	$[(\eta^6\text{-C}_6\text{H}_3\text{Me}_3)_2\text{Ru}]^{2+}$	-0.75 ^a
2b ^b	$\sim 18\,520$	~ 2.30	2170, 2187	$[(\eta^6\text{-C}_6\text{Me}_6)_2\text{Ru}]^{2+}$	-1.01 ^d
$[\text{Bu}_4\text{N}][\text{C}_6(\text{CN})_6]$			2194, 2208		+0.43 ^c
$[\text{Bu}_4\text{N}]_2[\text{C}_6(\text{CN})_6]$			2164, 2183		+0.43 ^c

^a Since the reversible redox potentials for these cations could not be determined due to the irreversible nature of the reduction, ΔE_{redox} was estimated from the difference in the peak potentials. The difference is equivalent to ΔE_{redox} for the $[(\eta^6\text{-C}_6\text{Me}_6)_2\text{M}]^{2+}$ cations, and therefore the use of peak potentials appears valid. ^b A distinct maximum could not be readily determined for the CT transition. ^c Reversible reduction potential for the $[\text{C}_6(\text{CN})_6]^{2-}/[\text{C}_6(\text{CN})_6]^{-}$ couple. ^d See ref 31.

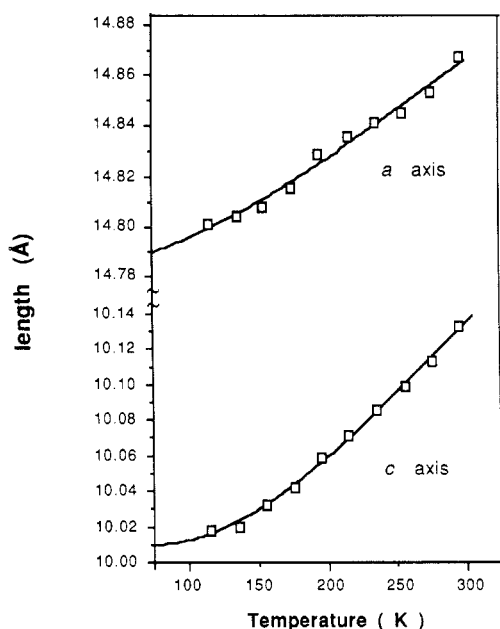


Figure 4. Temperature dependence of the unit cell lengths of 2a. The change in the length of the 1-D c axis is approximately twice that of the a axis over the same temperature range.

The mixed-stack arrangements and small interplanar distances (i.e., <3.30 Å) in 1a and 2a are reminiscent of those observed in mixed-stack organic DA solids,²⁴⁻²⁵ as well as in the organometallic charge-transfer complex $[(\eta^5\text{-C}_5\text{H}_5)_2\text{Fe}][\text{TCNE}]$.^{28,29} Charge-transfer interactions are apparent from the rather intense optical absorptions (Table IV) in 1a and 2a that occur in the visible spectra and are not present in either $[(\eta^6\text{-C}_6\text{Me}_3\text{H}_3)_2\text{M}]^{2+}$ or $[\text{C}_6(\text{CN})_6]^{2-}$. The rather small shifts in ν_{CN} of the HTMCP anion upon complex formation indicated that the anion in 1a and 2a more closely resembled the parent dianion than the monoanion. Therefore these solids are best described as weak DA complexes possessing "superionic"¹⁷ ground states with nominally doubly charged donors and acceptors and singly charged ionic excited states. This is consistent with electrochemical measurements which indicate that the $[\text{C}_6(\text{CN})_6]^{2-}$ anion undergoes a reversible oxidation to the monoanion¹⁶ at potentials that are much more positive than those required for $[(\eta^6\text{-C}_6\text{Me}_3\text{H}_3)_2\text{M}]^{2+}$ reduction (Table IV); i.e., complete electron transfer from

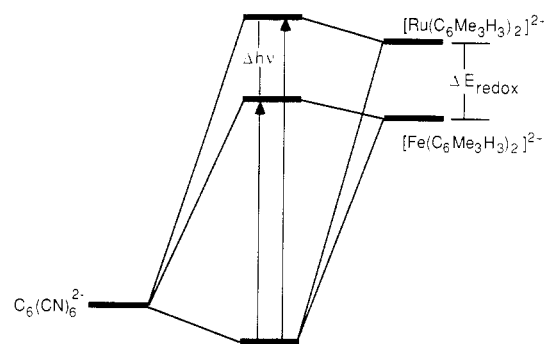


Figure 5. Schematic of the orbital mixing resulting from CT interaction in 1a and 2a. The observed difference in the CT transition energies ($\Delta h\nu_{\text{CT}}$) is equivalent to the difference in the measured reduction potentials ($\Delta E_{\text{redox}} = 0.77$ eV).

the dianion to the dication is not thermodynamically favored. However, the redox behavior of these species suggests that the dianion assumes the role as the donor and the organometallic dication the role as the acceptor. The wave functions for the ground and excited states can be represented by eq 2 and 3, where $\Psi_0(D^2-A^{2+})$ and $\Psi_1(D^-A^+)$ are the contributions from the noninteracting ions and ion pairs in which complete electron transfer has occurred, respectively. These states are analogous to the "no-bond" and "dative" terms used to describe neutral organic CT solids. The charge-transfer transition is therefore tantamount to electron transfer from $[\text{C}_6(\text{CN})_6]^{2-}$ to $[(\eta^6\text{-C}_6\text{Me}_3\text{H}_3)_2\text{M}]^{2+}$ (Figure 5).

$$\Psi_g = a\Psi_0(D^2-A^{2+}) + b\Psi_1(D^-A^+) \quad (2)$$

$$\Psi_e = a\Psi_0(D^-A^+) - b\Psi_1(D^2-A^{2+}) \quad (3)$$

The assignment of the observed visible absorptions as charge-transfer absorptions was corroborated by their observed dependence on the identity of the organometallic acceptor. For a given donor and constant Madelung terms, a decrease in the electron affinity (E_A) of the acceptor should result in an equivalent increase of the charge-transfer absorption energy.³⁰ A higher CT transition energy was therefore observed for 2a, since the E_A of $[(\eta^6\text{-C}_6\text{Me}_3\text{H}_3)_2\text{M}]^{2+}$ was suggested by the reduction potentials of the cations to be less when $M = \text{Ru}$. Interestingly, the difference in the CT absorption energies ($\Delta h\nu_{\text{CT}}$) of 1a and 2a was equivalent to the measured difference in reduction potential ($\Delta E_{\text{redox}} = 0.77$ eV) of the cations in solution³¹ (Figure 5). Although correlations have been made,³² agreements between these quantities are

(24) Dunitz, J. D.; Ibers, J. A. *Perspectives in Structural Chemistry*; Wiley: New York, 1971; Vol. IV.

(25) Soos, Z. G. *Annu. Rev. Phys. Chem.* 1974, 25, 121.

(26) Offen, H. W. *J. Chem. Phys.* 1965, 42, 430.

(27) Mayerle, J. J.; Torrance, J. B.; Crowley, J. I. *Acta Crystallogr., Sect. B: Struct. Crystallogr. Cryst. Chem.* 1979, B35, 2988.

(28) Adman, E.; Rosenblum, M.; Sullivan, S.; Margulis, T. N. *J. Am. Chem. Soc.* 1967, 89, 4540.

(29) Sullivan, B. W.; Foxman, B. M. *Organometallics* 1983, 2, 187.

(30) Mulliken, R. S. *J. Phys. Chem.* 1952, 56, 801.

(31) For elimination of errors, the reduction potentials of the cations were determined simultaneously in acetonitrile containing 0.2 M $[\text{Bu}_4\text{N}][\text{BF}_4]$. Although the reduction of the ruthenium cation has been shown to be a two-electron process,¹⁶ it is reasonable to assume that E° reflects the redox potential for transfer of the first electron.

generally not precise owing to inequivalent contributions to solvation and Madelung terms by different donors or acceptors. These results suggest that the presence of isostructural ligand environments in **1a** and **2a** mitigates against differences in solvation terms associated with redox processes as well as differences in Madelung energies in the solid state and that the difference in the E_A values of the cations can therefore be determined from the difference in their reduction potentials with reasonable accuracy. To our knowledge, this is the first example of such precise agreement between ΔE_{redox} and $\Delta h\nu_{\text{CT}}$ in DA solids attained by substitution of isostructural homologous components. This principle can be extended to other systems, as we have observed identical behavior in the DA solid $[(\eta^6\text{-C}_6\text{Me}_6)_2\text{M}][\text{iso-C}_4(\text{CN})_6]$ ($\text{M} = \text{Fe}, \text{Ru}$).³³

Agreement between ΔE_{redox} and $\Delta h\nu_{\text{CT}}$ was also found for **1b** and **2b**, although this agreement is not considered to be as reliable since λ_{max} of the CT absorption of **2b** was not easily discernible. The smaller CT transition energies observed for **1b** and **2b** compared to those of their mesitylene analogues were contrary to expectations based solely on comparison of the reduction potentials, as the more negative reduction potentials of $[(\eta^6\text{-C}_6\text{Me}_6)_2\text{M}]^{2+}$ suggested smaller electron affinities. This discrepancy demonstrates the importance of Madelung and solvation energies when comparing ΔE_{redox} and $\Delta h\nu_{\text{CT}}$ when the components possess different ligand environments and the solid-state structures are unknown.

The ν_{CN} values of the HMTCP anion in **1a** and **2a** were shifted slightly compared to the parent dianion to higher energy (toward ν_{CN} for the monoanion), suggesting contribution of the D^-A^+ term to the ground state. The extent of charge-transfer interaction, or excited-state mixing, in the ground state of DA solids is commonly estimated from shifts in vibrational frequencies of functional groups belonging to the components, assuming a linear relationship between the degree of charge transfer and the vibrational frequencies.^{34,35} If a similar analysis is employed for **1a** and **2a**, using eq 4³⁵ where b^2 is the degree of charge

$$b^2 = (\nu_d^2 - \nu_c^2) / (\nu_d^2 - \nu_m^2) \quad (4)$$

transfer, ν_d the vibrational frequency of the dianion, ν_c the frequency of the complex, and ν_m the frequency of the monoanion, the degree of charge transfer from the anion to the cation estimated from the lower and higher frequency ν_{CN} bands is 17 and 19%, respectively. However, identical values of b^2 were observed for **1a** and **2a**, which is inconsistent with the different electron affinities of the cations. The shifts in ν_{CN} may be due to the short $\text{C}\equiv\text{N}$ bond lengths induced by the close interstack contacts between the anion nitrogen atoms and mesitylene ligands (vide supra). Although it is possible that the effect of different electron affinities on vibrational frequencies is too small to be observed, these results illustrate that caution must be exercised when evaluating the extent of excited-state mixing from vibrational frequencies in DA solids due to presence of solid-state and electrostatic effects.

The presence of planar aromatic ring ligands that essentially encapsulate the metal atom (as seen from molecular models) in the $[(\eta^6\text{-arene})_2\text{M}]^{2+}$ cations suggests that

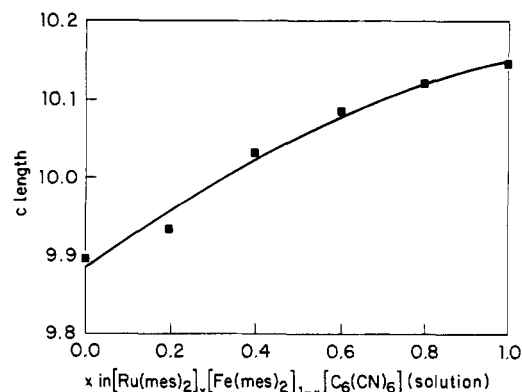


Figure 6. (a) Dependence of the c axis length on the amount of $[(\eta^6\text{-C}_6\text{Me}_3\text{H}_3)_2\text{Ru}]^{2+}$ in solution during crystallization of the mixed-metal complexes. The slight deviation from linearity is consistent with a small degree of ruthenium enrichment in the mixed phases.

these solids resemble organic DA solids. However, electronically they may be very different due to the influence of the metal orbitals, as is apparent from the different redox potentials observed for the different cations and the different CT energies of the complexes. In order for these complexes to be considered as analogues of organic solids, the excited state should preferably be localized on the arene ligands. Although the assignment of the LUMO is unclear, previous reports that cite the presence of low-lying ligand orbitals in $[(\eta^6\text{-arene})_2\text{M}]^{2+}$ suggest this is plausible. The unoccupied metal e_{1g}^* (d_{xz}, d_{yz}) and ligand e_{2u}^* (p_z) orbitals may be very close in energy,^{36,37} and extensive mixing of e_{2u}^* into the metal orbitals was also noted.^{38,39} The exact orbital ordering is presently difficult to establish as it is very sensitive to charge as well as substitution on the arene rings, as shown by the systematic cathodic shift in reduction potential as methyl group substitution increases.⁴⁰ However, the observation that the C_6H_6 ring of $[(\eta^6\text{-C}_6\text{H}_6)\text{Ru}(\eta^6\text{-C}_6\text{Me}_3\text{H}_3)]^{2+}$ is readily attacked by hydride⁴¹ is consistent with the presence of a low-lying ligand orbital. The overlap of the $[\text{C}_6(\text{CN})_6]^{2-}$ anion with the ring carbon atoms of the mesitylene ligands and the short interplanar separation between ions are also suggestive of electronic interactions with the ligands. However, we have observed that $[(\eta^6\text{-C}_6\text{Me}_3\text{H}_3)_2\text{Fe}][\text{C}_6(\text{CN})_6]_2$ does not exhibit face-to-face stacking of the ions.¹⁸ This suggests that electrostatic attractions between the highly charged ions may be an important consideration in the stacking motif and small interplanar separation observed in these solids. Theoretical investigations are currently in progress to elucidate the nature of the CT interactions.⁴²

Solid Solutions. Crystallization from solutions containing both $[(\eta^6\text{-C}_6\text{Me}_3\text{H}_3)_2\text{Fe}]^{2+}$ and $[(\eta^6\text{-C}_6\text{Me}_3\text{H}_3)_2\text{Ru}]^{2+}$ gave well-formed single crystals of $[(\eta^6\text{-C}_6\text{Me}_3\text{H}_3)_2\text{Ru}]_x\text{-}[(\eta^6\text{-C}_6\text{Me}_3\text{H}_3)_2\text{Fe}]_{1-x}[\text{C}_6(\text{CN})_6]$. Alternatively, these mixed-metal phases can be prepared electrochemically by potentiostatic reduction of $[\text{C}_6(\text{CN})_6]^-$ in the presence of

(32) Torrance, J. B.; Vasquez, J. E.; Mayerle, J. J.; Lee, V. Y. *Phys. Rev. Lett.* **1981**, *46*, 253.

(33) Ward, M. D., to be submitted for publication.

(34) Van Duyne, R. P.; Cape, T. W.; Suchanski, M. R.; Siedle, A. R. *J. Phys. Chem.* **1986**, *90*, 739.

(35) Friedrich, H. B.; Person, W. B. *J. Chem. Phys.* **1966**, *44*, 2161. Jurgensen, C. W.; Peanasky, M. J.; Drickamer, H. G. *J. Chem. Phys.* **1985**, *83*, 6108.

(36) (a) Anderson, S. E., Jr.; Drago, R. S. *Inorg. Chem.* **1972**, *11*, 1564.

(b) Clack, D. W.; Warren, K. D. *J. Organomet. Chem.* **1978**, *152*, C60.

(37) Brintzinger, H.; Palmer, G.; Sands, R. H. *J. Am. Chem. Soc.* **1965**, *87*, 623.

(38) Morrison, W. H.; Ho, E. Y.; Hendrickson, D. N. *Inorg. Chem.* **1975**, *14*, 500.

(39) Anderson, S. E., Jr.; Drago, R. S. *J. Am. Chem. Soc.* **1970**, *92*, 4244.

(40) Hamon, J. R.; Astruc, D.; Michaud, P. *J. Am. Chem. Soc.* **1981**, *103*, 758.

(41) Rybinskaya, M. I.; Kaganovich, V. S.; Kudinov, A. R. *J. Organomet. Chem.* **1982**, *235*, 215.

(42) Dixon, D. A.; Ward, M. D., work in progress.

both cations. Comparison of room-temperature unit cell constants of **1a** and **2a** reveals that the *a* and *b* axes (perpendicular to the 1-D axes) are identical (**1a**, 14.875 Å; **2a**, 14.876 Å). However, the length of the 1-D *c* axis of **2a** (10.145 Å) is 0.28 Å longer than that of **1a** (9.858 Å), which is equivalent to the difference between the intramolecular mesitylene-mesitylene distances. The dimensions perpendicular to the 1-D axes are determined by the hydrocarbon framework whereas the length of the linear chain is affected by the larger radius of Ru^{II} compared to that of Fe^{II}.¹⁹ Consequently, the *a* axis length determined for the mixed-metal phases by X-ray powder diffraction methods did not vary for different values of *x* for $0 \leq x \leq 1$, but the *c* axis length increased monotonically with increasing amounts of ruthenium in solution (Figure 6). The dependence of the *c* axis length on *x* in the mixed-metal phases is consistent with Vegard's law,⁴³ which predicts a linear relation between measured lattice constants and composition of solid-solution alloys expressed as relative concentrations of the components. Single-crystal unit cell determinations were in agreement with these results. For example, a crystal retrieved from a solution that contained equimolar amounts of $[(\eta^6\text{-C}_6\text{Me}_3\text{H}_3)_2\text{Fe}]^{2+}$ and $[(\eta^6\text{-C}_6\text{Me}_3\text{H}_3)_2\text{Ru}]^{2+}$ exhibited a unit cell length of 10.013 (5) Å, which suggested $x = 0.54 \pm 0.02$. The diffraction lines of the mixed-metal single crystals were broader than those of the single metal phases. Elemental analysis of crystals obtained from the same batch indicated that $x = 0.49 \pm 0.03$ and analysis of single crystals by X-ray fluorescence electron microprobe gave $x = 0.55 \pm 0.06$. Microprobe analysis of cross sections obtained by cleaving crystals perpendicular to the long axis (which is coincident with the *c* axis) showed that iron and ruthenium were uniformly distributed throughout the crystals. Therefore, the mixed-metal phases can best be described as solid solutions containing mixed-metal linear chains with randomly incorporated DA pairs. The mixed-metal complexes always exhibited slight enrichment of ruthenium when compared to the initial solution concentrations, as suggested from the slight deviation from linearity in Figure 6. Although this may reflect different crystallization kinetics of the cations, it is believed to be due to a small degree of decomposition of $[(\eta^6\text{-C}_6\text{Me}_3\text{H}_3)_2\text{Fe}]^{2+}$, which lowers its concentration during crystallization. The results indicate that the growing crystal does not discriminate between either cation; presumably the isostructural framework that results in only a small difference in the axial length of the cation allows random incorporation of these species.

The optical properties of the mixed-metal phases differed significantly from the parent complexes, as the relative intensities of the CT absorptions were dependent upon the relative amounts of ruthenium and iron in the complex (Figure 7). As a result of solid-solution formation and the subsequent contribution of CT bands from both chromophores, the colors of these mixed phases vary with the value of *x*. When care was taken to ensure that equivalent areas of pellets of these complexes were sampled during acquisition of UV-vis diffuse reflectance spectra, an isosbestic point was observed. This is consistent with Beer's law behavior and the presence of noninteracting localized chromophores. For example, when $x = 0.5$, green single crystals are obtained. Only the macroscopic properties of the crystal were altered as no evidence for the formation of new band structures was observed. Although small shifts in the maxima of the charge-transfer bands

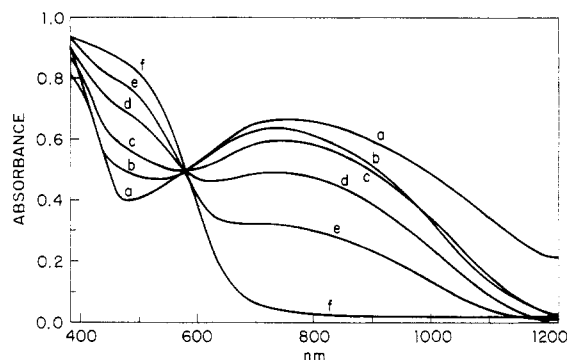


Figure 7. Diffuse reflectance spectra of $[(\eta^6\text{-C}_6\text{Me}_3\text{H}_3)_2\text{Ru}]_x\text{-}[(\eta^6\text{-C}_6\text{Me}_3\text{H}_3)_2\text{Fe}]_{1-x}[\text{C}_6(\text{CN})_6]_2$: (a) $x = 0$; (b) $x = 0.2$; (c) $x = 0.4$; (d) $x = 0.6$; (e) $x = 0.8$; (f) $x = 1.0$.

would be difficult to observe owing to their broadness, the absence of any appreciable shift or new bands suggests little electronic interaction between DA ion pairs and is consistent with the absence of any band structure in these solids. Mixed-stack charge-transfer solids generally do not display any evidence of extended band structure, although delocalization of the charge-transfer transition over several centers has been proposed for Magnus' green salt, $[\text{Pt}(\text{NH}_3)_4][\text{PtCl}_4]$.⁴⁴

To our knowledge, this is the first example of property modification by solid-solution formation in a mixed-stack DA complex, although a few examples of other low-dimensional solid solutions have been reported. For example, the degree of band filling in segregated-stack solids was controlled by variation of *x* in $(\text{NMP})_{1-x}(\text{Phen})_x\text{-}(\text{TCNQ})$ [NMP = *N*-methylphenazinium; Phen = phenazine; TCNQ = tetracyanoquinodimethane],⁴⁵ and solid solutions of $(\text{TSeF})_x(\text{TTF})_{1-x}(\text{TCNQ})$ (TSeF = tetrasele- nifulvalene; TTF = tetrathiafulvalene) were reported to exhibit electronic properties that differed from the parent complexes.⁴⁶ While not rigorously solid solutions, organometallic quasi-racemates based on dicarbonylrhodium(I) (*1S*)-3-trifluoroacetylcamphorate, and dicarbonyliridium(I) (*1R*)-3-trifluoroacetylcamphorate complexes were reported which possessed ordered alternating (Rh,Rh,Ir,Ir)_∞ columnar structures.⁴⁷ Although detailed optical data was not reported, the quasi-racemate exhibited a color different than its quasi-enantiomers.

Concluding Remarks

Coulombic interactions play an important role in the properties of low-dimensional DA solids. Lattice compression along the 1-D axis can result in barochromism⁴⁸ and thermochromism⁴⁹ due to differences in Madelung energies of the ground and excited states.^{50,51} The difference in Madelung energies of ground and excited states in "superionic" DA solids such as **1** and **2** is potentially much more significant than in neutral or ionic complexes. Preliminary investigations of the physical properties of **1**

(44) Anex, B. G.; Foster, S. I.; Fucaloro, A. F. *Chem. Phys. Lett.* **1973**, *18*, 126.

(45) Miller, J. S.; Epstein, A. J. *J. Am. Chem. Soc.* **1978**, *100*, 1639. Miller, J. S.; Epstein, A. J. *Angew. Chem.*, in press.

(46) Engler, E. M.; Scott, B. A.; Etemad, S.; Penney, T.; Patel, V. V. *J. Am. Chem. Soc.* **1977**, *99*, 5909.

(47) Schurig, V.; Pille, W.; Winter, W. *Angew. Chem., Int. Ed. Engl.* **1981**, *20*, 807.

(48) Bentley, W. H.; Drickamer, H. G. *J. Chem. Phys.* **1965**, *42*, 1573.

(49) Batail, P.; LaPlaca, S. J.; Mayerle, J. J.; Torrance, J. B. *J. Am. Chem. Soc.* **1981**, *103*, 951.

(50) Metzger, R. M.; Torrance, J. B. *J. Am. Chem. Soc.* **1985**, *107*, 117.

(51) Torrance, J. B. *Mol. Cryst. Liq. Cryst.* **1985**, *126*, 55.

(43) Vegard, L. Z. *Phys.* **1921**, *5*, 17.

Table V. Experimental Details for $[(\eta^6\text{-C}_6\text{Me}_3\text{H}_3)_2\text{M}][\text{C}_6(\text{CN})_6]$ (M = Fe, Ru) Complexes

	1a	2a
mol formula	$\text{C}_{30}\text{H}_{24}\text{N}_6\text{Fe}$	$\text{C}_{30}\text{H}_{24}\text{N}_6\text{Ru}$
fw	524.21	569.64
cryst. dimens., mm	$0.20 \times 0.25 \times 0.30$	$0.32 \times 0.38 \times 0.45$
peak width at half-height, deg	0.20	0.33
source	Mo $K\alpha$ radiation ($\lambda = 0.71073 \text{ \AA}$)	Cu $K\alpha$ ($\lambda = 1.54184 \text{ \AA}$)
temp, °C	23 ± 1	-35 ± 1
space group	$R\bar{3}$	$R\bar{3}$
a, Å	14.875 (5)	14.825 (5)
c, Å	9.858 (4)	10.093 (3)
V, Å ³	1889 (2)	1921 (2)
Z, g/cm ³	1.38	1.48
μ , cm ⁻¹	6.5	52.9
solution	direct methods	patterson method
hydrogen atoms	included in calcd positions	refined with $B_{\text{iso}} = 5.0 \text{ \AA}^2$
anomalous dispersn	all non-hydrogen atoms	all non-hydrogen atoms
reflectns included	575 with $F_o^2 > 3.0\sigma(F_o^2)$	602 with $F_o^2 > 2.0\sigma(F_o^2)$
parameters refined	91	87
unweighted agreement factor	0.047	0.026
weighted agreement factor	0.056	0.031
esd of observn of unit weight	1.17	2.27
convergence, largest shift	0.01 σ	0.02 σ
high peak in final diff map, e/Å ³	0.55	0.41 (6)
instrument	Enraf-Nonius CAD4 diffractometer	Enraf-Nonius CAD4 diffractometer
monochromator	graphite crystal, incident beam	graphite crystal, incident beam
attenuator	Zr foil, factor 20.7	Ni foil, factor 21.1
takeoff angle, deg	2.8	2.8
detector aperture, mm	2.0–2.5 horizontal, 2.0 vertical	2.0–3.7 horizontal, 4.0 vertical
crystal-detector dist, cm	21	21
scan type	ω - θ	ω - θ
scan rate, deg/min	2–20 (in Ω)	2–5 (in Ω)
scan width, deg	$0.7 + 0.35 \tan \theta$	$0.8 + 0.140 \tan \theta$
max 2θ , deg	60.0	120.0
no. of reflectns measd	1348 total, 1221 unique	1665 total, 602 unique
correctns	Lorentz-polarization	Lorentz-polarization, linear decay (from 0.978 to 1.143 on I) reflection averaging (agreement on I = 2.2%)

and 2 have revealed a pronounced thermochromism with the direction of the shift to higher energy,⁵² presumably induced by the lattice contraction observed upon cooling. Interestingly, the direction of this shift is opposite to that normally observed for neutral organic CT complexes.^{53,54} This is believed to be a manifestation of the doubly charged ground state, which is stabilized to a greater extent than the singly charged excited state as the distance between the oppositely charged constituents decreases. Details of the environmental effects on these complexes will be presented in a future publication.

The DA complexes described above illustrate of the advantages of organometallic reagents in the design of molecular solids and their properties. The $[(\eta^6\text{-C}_6\text{Me}_3\text{H}_3)_2\text{M}]^{2+}$ cations structurally resemble organic aromatic dications, lending insight into solid-state aspects of a hypothetical class of DA solids. Furthermore, the microscopic optical properties can be rationally modified by altering the electron affinity of the organometallic acceptor species through homologous substitution of the metal atom. The isostructural nature of the acceptor cations allows accurate prediction of the change in the CT transition energy from reduction potentials due to small differences in Madelung and solvation energies. It also allows the synthesis of solid solutions in which one can "tune" the optical response of the bulk solids. Methods such as these may prove valuable in the design of molecular solids for electronic devices. It is envisioned that other "organometallic alloys" can be prepared by similar methods, provided isomorphism and near equivalent unit cell parameters in at least two dimensions are present. Given

the wealth of organometallic complexes, this promises to result in the design of new materials with interesting properties.

Experimental Section

Materials. Acetonitrile was distilled from CaH_2 under nitrogen and nitromethane from CaSO_4 under nitrogen. Tetra-*n*-butylammonium tetrafluoroborate was recrystallized from ethyl acetate-ethanol and dried in vacuo prior to use. Literature methods were used for the preparation of $[(\eta^6\text{-arene})_2\text{Fe}][\text{PF}_6]_2$,¹⁰ $[(\eta^6\text{-arene})_2\text{Ru}][\text{BF}_4]_2$,¹¹ and $[\text{Bu}_4\text{N}]_2[\text{C}_6(\text{CN})_6]$.¹⁶

Equipment. All manipulations were performed under inert atmosphere conditions by using purified nitrogen and a Vacuum Atmospheres glovebox. Reduction potentials were determined by cyclic voltammetry with a Princeton Applied Research 173 potentiostat using platinum working and auxiliary electrodes and an Ag/AgCl reference electrode purchased from Bio-Analytical Systems, Inc., in a standard H-cell with a glass fritted separator. Electrocrystallizations were performed with identical equipment using platinum foil ($0.5 \times 0.5 \text{ cm}$) as the working electrode. Infrared spectra were recorded on a Nicolet 7199 Fourier transform spectrometer. The UV-visible diffuse reflectance spectra were recorded on a Cary 2390 spectrometer.

Synthesis of $[(\eta^6\text{-C}_6\text{Me}_3\text{H}_3)_2\text{Fe}][\text{C}_6(\text{CN})_6]$ (1a). Under nitrogen, a solution of $[(\eta^6\text{-C}_6\text{Me}_3\text{H}_3)_2\text{Fe}][\text{PF}_6]_2$ (59 mg, 0.1 mmol) in 10 mL of acetonitrile was slowly added to a solution of $[\text{Bu}_4\text{N}]_2[\text{C}_6(\text{CN})_6]$ (72 mg, 0.1 mmol) in 10 mL of acetonitrile, upon which a blue precipitate was immediately observed. Filtration of the mixture followed by several washings with acetonitrile gave 1a in quantitative yield. Anal. Found: C, 68.34; H, 4.72; N, 15.69. Calcd: C, 68.71; H, 4.61; N, 16.03. Similar procedures were used for the preparation of $[(\eta^6\text{-C}_6\text{Me}_3\text{H}_3)_2\text{Fe}][\text{C}_6(\text{CN})_6]$ (1b) using $[(\eta^6\text{-C}_6\text{Me}_3\text{H}_3)_2\text{Fe}][\text{PF}_6]_2$ (67 mg, 0.1 mmol). Anal. Found: C, 70.73; H, 5.86; N, 13.91. Calcd: C, 71.06; H, 5.96; N, 13.81.

Synthesis of $[(\eta^6\text{-C}_6\text{Me}_3\text{H}_3)_2\text{Ru}][\text{C}_6(\text{CN})_6]$ (2a). Under nitrogen, a solution of $[(\eta^6\text{-C}_6\text{Me}_3\text{H}_3)_2\text{Ru}][\text{BF}_4]_2$ (51 mg, 0.1 mmol) in 10 mL of acetonitrile was slowly added to solution of $[\text{Bu}_4\text{N}]_2[\text{C}_6(\text{CN})_6]$ (72 mg, 0.1 mmol) in 10 mL of acetonitrile, upon

(52) Caspar, J. V.; Ward, M. D., unpublished results.

(53) Offen, H. W. *J. Chem. Phys.* 1965, 42, 430.

(54) Hammond, P. R.; Burkhardt, L. A. *J. Phys. Chem.* 1970, 74, 639.

which an orange-red precipitate was immediately observed. Filtration of the mixture followed by several washings with acetonitrile gave **2a** in quantitative yield. Anal. Found: C, 62.75; H, 4.24; N, 14.17. Calcd: C, 63.36; H, 4.25; N, 14.75. Similar procedures were used for the preparation of $[(\eta^6\text{-C}_6\text{Me}_6)_2\text{Ru}][\text{C}_6(\text{CN})_6]$ (**2b**) using $[(\eta^6\text{-C}_6\text{Me}_6)_2\text{Ru}][\text{BF}_4]_2$ (67 mg, 0.1 mmol). Anal. Found: C, 65.42; H, 5.66; N, 12.40. Calcd: C, 66.14; H, 5.55; N, 12.85.

Procedures for Crystal Growth. Crystals for single-crystal X-ray structure determinations were prepared by slow diffusion techniques in three-chambered cells in which the chambers were separated by medium porosity fritted glass. Crystal growth was accomplished with either acetonitrile or nitromethane as solvent, although the latter generally yielded crystals of higher quality. The following procedure for the synthesis of **1a** is exemplary. Nitromethane solutions containing 0.01 M $[(\eta^6\text{-C}_6\text{Me}_3\text{H}_3)_2\text{Fe}][\text{PF}_6]_2$ and 0.01 M $[\text{Bu}_4\text{N}]_2[\text{C}_6(\text{CN})_6]$ were added to the separate outer compartments of a three-chambered cell. Neat solvent was then added to the center chamber. After the cell was left to stand for 2 weeks at 10 °C under nitrogen, dark blue needles of **1a** were harvested from the center chamber and washed with nitromethane.

Electrocrystallization of $[(\eta^6\text{-Arene})_2\text{M}][\text{C}_6(\text{CN})_6]$. Complexes **1** and **2** were prepared electrochemically by reduction of $[\text{C}_6(\text{CN})_6]^-$ in the presence of the appropriate cation. The following procedure for the synthesis of **2a** is exemplary. An acetonitrile solution with 0.02 M $[\text{Bu}_4\text{N}][\text{C}_6(\text{CN})_6]$, 0.01 M $[(\eta^6\text{-C}_6\text{Me}_3\text{H}_3)_2\text{Ru}][\text{BF}_4]_2$, and 0.1 M Bu_4NBF_4 was added to the working compartment of a standard H-cell with a fritted-glass separator and an acetonitrile solution with 0.1 M Bu_4NBF_4 added to the auxiliary compartment. The potential of the working platinum electrode was held at +0.2 V (vs. Ag/AgCl) for 4 days. Filtration of the solution gave **2a** in quantitative Faradaic yield.

Preparation of Mixed-Metal Phases $[(\eta^6\text{-C}_6\text{Me}_3\text{H}_3)_2\text{Ru}]_x[(\eta^6\text{-C}_6\text{Me}_3\text{H}_3)_2\text{Fe}]_{1-x}[\text{C}_6(\text{CN})_6]$. Single crystals of the mixed-metal phases were also prepared in three-chambered crystallization cells. The following procedure for the synthesis for $x = 0.4$ is exemplary. Acetonitrile was the preferred solvent for growth of these phases. An acetonitrile solution containing 4 mM $[(\eta^6\text{-C}_6\text{Me}_3\text{H}_3)_2\text{Ru}][\text{BF}_4]_2$ and 6 mM $[(\eta^6\text{-C}_6\text{Me}_3\text{H}_3)_2\text{Fe}][\text{PF}_6]_2$ was added to one chamber of a three-chambered crystallization cell. To the other outer compartment was added 10 mM $[\text{Bu}_4\text{N}]_2[\text{C}_6(\text{CN})_6]$. Neat solvent was then added to the center chamber. After the cell was left to stand for 2 weeks at 10 °C under nitrogen, dark green needles were harvested from the center chamber and washed with nitromethane. The mixed-metal phases can also be prepared electrochemically by a procedure similar to that described above for **2a**. The value of x is controlled by the relative amounts of $[(\eta^6\text{-C}_6\text{Me}_3\text{H}_3)_2\text{Fe}][\text{PF}_6]_2$ and $[(\eta^6\text{-C}_6\text{Me}_3\text{H}_3)_2\text{Ru}][\text{BF}_4]_2$ in the working compartment.

X-ray Data Collection and Data Reduction.⁵⁵ Preliminary examination and data collection were performed on an Enraf-Nonius CAD4 computer-controlled κ axis diffractometer equipped with a graphite crystal, incident beam monochromator. Table V summarizes the relevant conditions of data collection.

Cell constants and an orientation matrix for data collection were obtained from least-squares refinement, using the setting angles of 25 reflections in the range $9 < \theta < 21^\circ$ for **1a** and 16 reflections in the range $15 < \theta < 25^\circ$ for **2a**, measured by the computer-controlled diagonal slit method of centering.

As a check on crystal and electronic stability three representative reflections were measured every 41 min for **1a** and every 30 min for **2a**. The intensities of these standards remained constant within experimental error throughout data collection

for **1a**, and no decay corrections were applied. An anisotropic decay correction was applied for **2a**, as given in Table V.

Structure Solution and Refinement. Relevant conditions are summarized in Table V. The structures were solved by either direct or Patterson methods. The structures were refined in full-matrix least-squares where the function minimized was $\sum w(|F_o| - |F_c|)^2$ and the weight w is defined as $4F_o^2/s^2(F_o^2)$. The standard deviation on intensities, $s^2(F_o^2) = [S^2(C + R^2B) + (pF_o^2)^2]/Lp^2$ where S is the scan rate, C is the total integrated peak count, R is the ratio of scan time to background counting time, B is the total background count, Lp is the Lorentz-polarization, factor, and the parameter p (ignorance factor) is a factor introduced to downweight intense reflections.

Scattering factors were taken from Cromer and Waber.⁵⁶ Anomalous dispersion effects were included in F_c ,⁵⁷ the values for $\Delta f'$ and $\Delta f''$ were those of Cromer.⁵⁸ Only the reflections having intensities greater than 3.0 times their standard deviation were used in the refinements. The final cycle of refinement converged with unweighted and weighted agreement factors of according to

$$R_1 = \sum(|F_o| - |F_c|) / \sum|F_o|$$

$$R_2 = (\sum w(|F_o| - |F_c|)^2 / \sum w F_o^2)^{1/2}$$

The height of the highest peak in the final difference Fourier and the estimated error based on ΔF ⁵⁹ are given in Table V. Plots of $\sum w(|F_o| - |F_c|)^2$ vs. $|F_o|$, reflection order in data collection, $\sin(\theta/\lambda)$, and various classes of indices showed no unusual trends for any of the compounds.

Acknowledgment. The author thanks J. S. Miller for bringing the hexacyanotrimethylenecyclopropane dianion to his attention and E. J. Delawski for technical assistance.

Registry No. **1a**, 106865-37-6; **1b**, 106865-38-7; **2a**, 106865-39-8; **2b**, 106865-40-1; $[(\eta^6\text{-C}_6\text{Me}_3\text{H}_3)_2\text{Fe}][\text{PF}_6]_2$, 31666-55-4; $[(\eta^6\text{-C}_6\text{Me}_6)_2\text{Fe}][\text{PF}_6]_2$, 53382-63-1; $[(\eta^6\text{-C}_6\text{Me}_3\text{H}_3)_2\text{Ru}][\text{BF}_4]_2$, 71825-70-2; $[(\eta^6\text{-C}_6\text{Me}_6)_2\text{Ru}][\text{BF}_4]_2$, 71861-31-9; $[\text{Bu}_4\text{N}]_2[\text{C}_6(\text{CN})_6]$, 106865-41-2; $[\text{Bu}_4\text{N}][\text{C}_6(\text{CN})_6]$, 58608-56-3.

Supplementary Material Available: X-ray structural reports for **1a** and **2a** that contain the following: an introduction for **1a**, descriptions of experimental procedures for **1a** and **2a** that include data collection, data reduction, and structure solution and refinement, tables of crystal data, intensity measurements, structure solution and refinement, positional and thermal parameters, general temperature factor expressions (U 's), bond distances, bond angles, and torsional angles for **1a** and **2a**, tables of intermolecular contacts up to 3.60 Å and least-squares plane for **1a**, a table of root-mean-square (rms) amplitudes of thermal vibrations for **2a**, drawings of a single cation and two half-occupancy anions and the unit cell and a stereoview of the unit cell, all of which show 50% probability ellipsoids, for **1a**, and drawings of a single Ru molecule and of single anion disorder, both of which show the labeling scheme, and the unit cell and a stereoview of the unit cell, both of which show 20% probability ellipsoids for **2a** (40 pages); tables of intensity data (structure factor tables) for **1a** and **2a** (9 pages). Ordering information is given on any current masthead page.

(56) Cromer, D. T.; Waber, J. T. *International Tables for X-Ray Crystallography*; The Kynoch Press: Birmingham, England, 1974; Vol. IV, Table 2.2B.

(57) Ibers, J. A.; Hamilton, W. C. *Acta Crystallogr.* 1964, 17, 781.

(58) Cromer, D. J. *International Tables for X-Ray Crystallography*; The Kynoch Press: Birmingham, England, 1974; Vol. IV, Table 2.3.1.

(59) Cruickshank, D. W. J. *Acta Crystallogr.* 1949, 2, 154.

(55) These services were performed by the Molecular Structure Corp. (**1a**) and Oneida Research Services, Inc. (**2a**).